JOURNAL OF APPLIED ELECTROCHEMISTRY 25 (1995) 6–14

Electrolyte wetting effects in the comparative polarization behaviour of the hydrogen evolution reaction at Ni–Mo–Cd electrodes in KF · 2HF and KOH · $2H_2O$ melts

L. GAO, S. Y. QIAN, B. E. CONWAY

Department of Chemistry, University of Ottawa, Ottawa, Ontario, Canada K1N 6N5

Received 22 February 1994; revised 5 June 1994

In the electrolyte process of fluorine production from KF · 2HF melts at 85° C, unusually high polarization arises both at the cell anodes (carbon) and cathodes (mild steel) at moderate current densities. The anomalous polarization behaviour in fluorine evolution at carbon anodes has been extensively studied but much less is known about the origin of hyperpolarization in hydrogen evolution at the cathodes. Here, the results of comparative polarization studies at a Ni–Mo–Cd composite cathode material in a KF · 2HF melt and a corresponding aquo-analogue melt of KOH · $2H_2O$ are reported. Large differences are observed which are attributed to the different wetting characteristics of these two melts at the interface of the Ni–Mo–Cd cathodes that are microporous. Such electrode material also offers a major improvement of cathode polarization over that at mild steel surfaces. Conclusions on wetting effects are based on: (i) a comparative determination of hydrogen-bubble contact angles at the electrode in the two melts and (ii) an evaluation of the double-layer capacitances of the electrode interfaces with the two melts as determined by the fast potential-relaxation method, at short times after current interruption. The apparent double-layer capacitances at a given electrode are very different in the two melts.

1. Introduction

In the electrolytic process of fluorine production from KF · 2HF melts at 85° C, unusually high polarization arises both at the cell anodes (carbon) and cathodes (mild–steel) at moderate current densities. The anomalous polarization behaviour in fluorine evolution at carbon anodes (the 'anode effect') has been extensively studied but much less is known about the origin of hyperpolarization in hydrogen evolution at the cathodes.

We have recently shown [1] that the cathodic hyperpolarization effect arises, in part, from local consumption of HF in the diffusion layer at the hydrogen-evolving cathode (mild steel) used in the fluorine-production cells and also in our previous laboratory experiments [1]. The effect does not simply arise on account of concentration polarization in the hydrogen evolution process but to a major amplification of that effect due to local solidification of the melt in a solid film at the electrode surface due to local diminution of HF concentration. This specific effect arises because the melt is operated at 85° C which is near a eutectic point, so that local consumption of HF causes a relatively rapid rise in melting point.

In addition to the above effect we have also found that sluggish detachment of hydrogen bubbles formed at the cathode in the KF · 2HF melt electrolyte is a further cause of high polarization at the cathode and erratic current fluctuations.

In the present work we have examined several aspects of this second source of cathode hyperpolarization as: (i) an investigation of the polarization behaviour in the hydrogen evolution reaction (HER) in the KF · 2HF melt comparatively with respect to that in the aquo-analogue melt, KOH · $2H_2O$; (ii) an evaluation of the difference of contact angles of individual hydrogen bubbles at electrode surfaces in the two melts at the same temperature and (iii) a determination of double-layer capacitance values at the two melt interfaces with a Ni–Mo–Cd high-area, porous composite electrode. The latter aspect of the work originated from the aim of investigating new electrode materials and structures that might lead to much improved cathode polarization in the operation of fluorine-production cells.

2. Experimental details

2.1. *Electrodeposited Ni–Mo–Cd composite electrodes*

A composite Ni(80 at %)–Mo(19 at %)–Cd(1 at %) electrocatalyst was prepared and investigated as an alternative to the mild steel cathode employed industrially in the electrolytic preparation of fluorine from

0021-891X

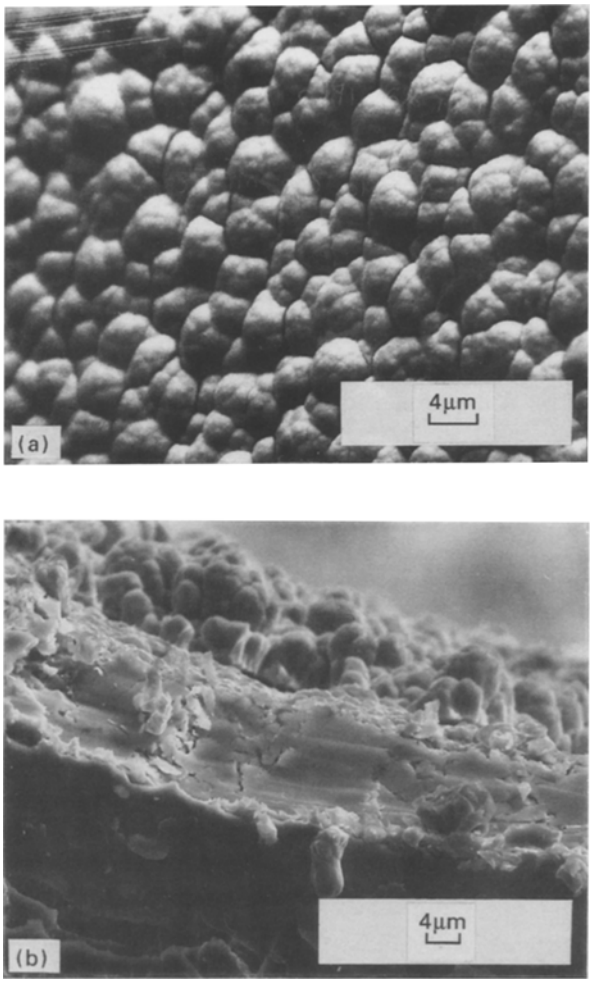

Fig. 1. SEM pictures of the electrodeposited Ni–Mo–Cd electrode: (a) top view; (b) sectional view.

KF · 2HF melts. The purpose of the alternative use of such materials is to achieve lower cathode polarization in the overall cell operation. In aqueous KOH, such Ni–Mo composites have been found [2] to give less than -100 mV overpotential at 100 mA cm^{-2} (apparent area). A cone-shaped electrode was designed to be used as a rotating electrode, which was found to be very effective for spinning off the gas bubbles generated at the electrode during the polarization which, in the KF · 2HF melt, otherwise adhere strongly to the electrode surface and raise the overvoltage by interference with local current distribution. The apparent surface area of the electrode was 0.28 cm^2. The electrodeposition of Ni–Mo–Cd proceeds easily on a mild steel rod substrate. The conditions for electroplating the composite coating have been previously described [2]. The electrode was rotated at 2000 r.p.m. during the plating process in order to spin off the simultaneously generated hydrogen gas.

The resulting composite electrode was examined under a scanning electron microscope (SEM); its surface appearance was 'cauliflower-like', with regions microporous in structure as shown in Fig. 1(a). The coating layer looks compact and fine. The deposited sample was then sliced vertically with the cut edge exposed. Figure 1(b) shows the SEM picture of this section plane. There are three layers in this deposit: the dark bottom part is the steel substrate, the middle layer is composed of the underlayer of electrodeposited Watts nickel (cf. [2]) and the top, 'cauliflower-like' layer is the Ni–Mo–Cd composite deposit. From the scale shown in this picture, it can be seen that the thickness of the total deposited layer is about 20 μm of which ca. 10 μm is from the contribution of the middle nickel layer. The mean composition of the alloy surface region was determined by X-ray emission analysis, giving the following actual atomic percentages: 88% Ni, 11% Mo and 0.25% Cd.

2.2. *Electrochemical cell*

Acrylic polymer is transparent (compared to Teflon) and resistive to acid and alkaline solutions and to HF; therefore it was selected as the material for fabrication of the cell for containing the KF · 2HF melt at 85° C.

An Fe/FeF$_2$ reference electrode was employed in the KF · 2HF melt and a Hg/HgO reference electrode in the KOH · 2H$_2$O hydrate solution. The relative potentials were measured experimentally referred to the RHE in the same system, and it was found that V_{Fe/FeF_2} against $V_{RHE} = 0.17$ V, and $V_{HgO/Hg}$ against $V_{RHE} = -0.91$ V at 85° C. Calibrations of overpotential were made according to these values in the comparative Tafel polarization experiments in the aqueous and the HF media.

A platinum gauze, having a large surface area, was used as the counter electrode in the aqueous solutions, while in the KF · 2HF melt, a graphite counter electrode (anode) had to be used, as is operated in industry for electrolytic fluorine production. The operating temperature, 85° C, in the experiment was maintained by an air-heated thermostat oven in which the cell was set up.

2.3. *KF · 2HF and KOH · 2H$_2$O melts*

Pure KF · 2HF (41% HF) melt, having a melting point of 71.7° C [3], was prepared from the 99+% KF · HF (solid) and 99.9% HF (gas) in a reaction of KF · HF + HF → KF · 2HF. Trace amounts of impurities can be present in the melt. Metal ion impurities (e.g. Fe^{3+}, Cu^{2+}) can be removed by prepolarization, while the moisture content (<0.1% H_2O) can be absorbed, when necessary, by adding small amounts of P_2O_5 to the melt without generating, it is believed, any new reactive products.

Aqueous KOH solutions, for the comparative experiments in the aquo-system, were made up from BDH 'Aristar' grade KOH and Milli-pore distilled water as solvent. The concentration of KOH · 2H$_2$O melt is estimated to be 28 M, i.e. without considering the activity factors for OH^- and H_2O.

2.4. *Technique of contact angle measurement*

Contact angle measurement is one of the useful

procedures that can be used for examination of adhesion in wetting of a solid surface by a liquid and is used to calculate adhesion tension. A contact angle goniometer (model 100, Kruss) was used to measure the angles of contact of hydrogen bubbles to the electrode in the melts. The hydrogen bubbles were generated *in situ* cathodically and recumbent bubbles could be viewed individually through the optical goniometer.

The melts were contained in the acrylic cell mounted in a chamber on the goniometer under controlled-temperature conditions. The gas/melt/electrode interphase was viewed through a microscope with rotatable reticules. The contact angle was measured from the aligned tangent of a fiducial hair to the bubble profile at its baseline of contact with the electrode substrate. The microscopic image was recorded photographically by a suitably mounted Polaroid camera.

2.5. *Electrochemical methods*

Steady-state polarization measurements were made utilizing an automated, computer-controlled data acquisition system developed in this laboratory, based on use of a Hokutu–Denko potentiostat. The results were plotted as Tafel relations, corrected for the effect of iR_s-drop due to the solution resistance, R_s; the latter was determined by the initial potential-relaxation method.

To derive information on double-layer capacitance and hence electrode surface area, open-circuit potential-relaxation transients (cf. [4, 5]) were recorded following the interruption of currents. Two Nicolet 310 oscilloscopes were used in tandem for data acquisition, starting in the microsecond region and covering times into the 10^1–10^2 s range. The acquired data in different timescales were treated and joined smoothly into one full curve. The fitting of initial transient curves was realized by the nonlinear regression method operated by means of STATGRAPH software [6, 7]. The procedures required for processing of the digitized potential-relaxation data were described in previous papers [5, 13, 14].

3. 'Acidity' of the KF · 2HF melt

Since the KF · 2HF melt is a nonaqueous electrolyte, little solvation energy is available to dissociate the HF bond, unlike the situation when it is in aqueous solutions. The strong H bond between HF and HF (H–F···HF) would further tend to minimize dissociation. Therefore, only a very small additional fraction of free ions would be expected in the melt arising from the self-dissociation, $2HF \rightleftharpoons H_2F^+ + F^-$, analogous to that in H_2O ($K_w = 10^{-14}$).

The 'acidity' of the KF · 2HF melt may be considered in relation to analogy with the aquo-system. Like H_2O, autoprotolysis in HF ($3HF \rightleftharpoons H_2F^+ + FHF^-$) is weak. The pH of the system is represented by $-\log[H_2F^+]$. Corresponding to KOH in the aquo-system, KF in HF is therefore an 'alkaline' solution, i.e. the KF · 2HF melt is actually to be regarded as an alkaline system in the HF solvent medium.

Although there is a clear chemical analogy between KF · 2HF in the 'HF system' and KOH · $2H_2O$ in the 'H_2O system', with regard to protonation equilibria and pH, KF · 2HF being 'alkaline' in the former system, it is not possible to make a quantitative comparison between the alkalinity of the two systems because the proton transfer energy between the two solvent media is not known and is likely to be moderately large. Related to this is the anticipated difference between the formal ionic products of the two media: $K_{H_2O} = [H_3O^+][OH^-]$ and $K_{HF} = [H_2F^+][FHF^-]$. However, intuitively, 'acidity' in the KF · 2HF system is likely to be substantially stronger than that of the KOH · $2H_2O$ system, based on the difference of conductivity of anhydrous HF and liquid H_2O.

4. Procedures for determination of C_{dl} from initial potential-relaxation transients

In evaluation of electrocatalyst materials and their performances in different media, it is essential to distinguish effects which arise just on account of real-area differences from other factors of more fundamental significance arising from electrode kinetic differences due to specific surface and electronic properties [8] of the electrode metals. Because of the practical importance of the accessible real-area of many electrocatalyst materials [9, 10], it is necessary to have ways of experimentally measuring *in situ* the 'real-area' factor independently of the overall activity. One of the major problems in *in situ* real surface area measurements is that there are difficulties in determining the real electrochemically active area, pertinent to the *overpotential* regions where significant Faradaic currents are passing and the utilized surface area may, in fact, be changing during the course of the electrode reaction. For example, in the process of metal plating, the surface area is usually continuously changing with time, while in the hydrogen evolution reaction at porous electrocatalysts, some fine pores may become filled by hydrogen gas as the electrolysis proceeds and/or wetting of the electrode material may change.

It is well known that determination of the double-layer capacitance C_{dl} or use of the Parsons–Zobel method [11] offers a relevant measurement of real areas of electrodes of simple geometry, based on some calibration value for the C_{dl} at a well-defined reference surface. On the other hand, gas/solid BET measurements of areas of porous materials, accessible to gases in the dry state, may not give values relevant to partially wetted surfaces of porous electrodes at which a continuous electrode process is taking place.

As may be expected, major difficulties in C_{dl} measurement can arise in the overpotential region and are associated with three problems: (i) the presence of the usually substantial continuous Faradaic

current that passes; (ii) the presence of the pseudocapacitance, C_ϕ [12], corresponding to the potential-dependence of adsorption of reaction intermediates (here H) and (iii) the influence of the porosity of the electrode on the distributed double-layer capacitance and resistance [10], which determines the internal current distribution and the response of the interface to alternating potential or pulse modulation.

These problems are dealt with in the present work by means of fast open-circuit potential-relaxation measurements, followed by interruption of the prior steady-state current. This method for *in situ* area measurement by C_{dl} determination has been quantitatively verified in recently published papers [13, 14] and proved to be reliable both on the basis of a theoretical treatment and from experimental results employing a prototype system involving porous platinum electrodes by comparison of cyclic voltammetry and a.c. impedance measurements; very good agreement was obtained from the results derived from several complementary techniques. The method was therefore applied to the systems under examination in the present work, and is based on the following principles.

For an electrode process, the dependence of current density, i, on overpotential, η, is represented in the usual way as

$$i(\eta) = i_0 \exp(\alpha\eta F/RT) \tag{2}$$

which is the Tafel equation in exponential form and where i_0 is the exchange current density and α the transfer coefficient.

The potential-relaxation relation, $\eta(t)$, after interruption of current, $i_{t=0}$, is determined by

$$-C(\mathrm{d}\eta/\mathrm{d}t) = i(\eta) = i_0 \exp(\alpha\eta F/RT) \tag{3}$$

where C is the interfacial capacitance ($C = C_{dl}$, if C_ϕ is negligible or not involved). This equation originates from the early treatment of Armstrong and Butler [4] for the case $C = C_{dl}$, e.g. for the HER at Hg; when C includes an adsorption pseudocapacitance arising from potential dependence of coverage, θ, of an intermediate, and θ is appreciable (e.g. $0.1 < \theta < 1$), the interpretation of potential-relaxation transients becomes more complex, but was thoroughly examined in [5] where it was shown that the presence of pseudocapacitance will *not* influence the C_{dl} determination, since the fitting of the *initial* region of the potential-relaxation transient involves only the potential response from the discharge of the double-layer capacitance over the short time domain, e.g. 1 μs – 1 ms (cf. [6, 7]).

Integration of Equation 3 (assuming that C is constant*) gives

$$\eta(t) = a - b\log(t + \tau) \tag{4}$$

where

$$a = -b\log(2.3 i_0/bC) \tag{5}$$

$$b = 2.3\,RT/\alpha F \tag{6}$$

and the integration constant, τ, is

$$\tau = bC/2.3 i_{t=0} \tag{7}$$

From Equation 3,

$$C_{dl} = i_{t=0}/(-\mathrm{d}\eta/\mathrm{d}t)_{t=0} \tag{8}$$

$i_{t=0}$ is measured experimentally at each potential for which current interruption is made. C_{dl}, corresponding to the interfacial capacitance at the overpotential $\eta(t=0)$, at which the initial current is passing, can be calculated from Equation 8 if the initial potential-relaxation slope $(-\mathrm{d}\eta/\mathrm{d}t)_{t=0}$ could be accurately evaluated; in our experience, this slope cannot be at all reliably obtained just by simply drawing a tangent to the η against t curve at $t = 0$.

It is possible, however, to proceed as follows by means of an extrapolation and curve-fitting procedure: differentiating Equation 4 with respect to t, gives

$$(-\mathrm{d}\eta/\mathrm{d}t)_{t=0} = -b/2.3\,\tau \;(\equiv -i_{t=0}/C) \tag{9}$$

Therefore, from the fitting of the initial region of a digitally recorded potential-relaxation curve, employing Equation 4, the parameters a, b and τ can be reliably obtained, and $(-\mathrm{d}\eta/\mathrm{d}t)_{t=0}$ then calculated from Equation 9, so that C_{dl} can be derived using Equation 8. It is to be emphasized that the curve-fitting procedure is not involved as an empirical basis for interpretation of the results but is used only to provide a sound basis (cf. [13, 14]) for extrapolation of $\eta(t)$ to $t = 0$ and evaluation of $(-\mathrm{d}\eta/\mathrm{d}t)_{t=0}$ using Equation 9.

5. Results and discussion

5.1. *Tafel polarization measurements*

Tafel polarization measurements were conducted on the HER at the Ni–Mo–Cd electrode in the KF · 2HF melt at 85° C. The results were compared with those at a mild steel electrode of the type used industrially in the commercial fluorine electrolytic process and plotted on the same graph (Fig. 2). The data designated by the plus (+) points are for the Ni–Mo–Cd rotating at 2000 r.p.m. and by the circle (○) points for the same electrode but stationary; (*) points are for the smooth mild steel cone electrode. For comparative purpose, results are also shown for a smooth, single-phase Ni(94 at %)–Mo(6 at %) alloy (× points). *IR* drop corrections have already been made in the Tafel plots shown.

First, it can be seen that the current densities at given potentials on the porous Ni–Mo–Cd electrode are about two magnitudes larger than that at the smooth mild steel electrode. This is a desired and major improvement in cathodic polarization in the HER from the KF · 2HF melt. One of the principal contributions to the enhanced catalytic performance

* It was found [8] that C_{dl} is, relatively speaking, a potential-independent quantity for the HER at Pt or Ni, although it is well known that C_{dl} may vary significantly with potential, especially around the potential of zero charge in dilute solutions, e.g. as at Hg.

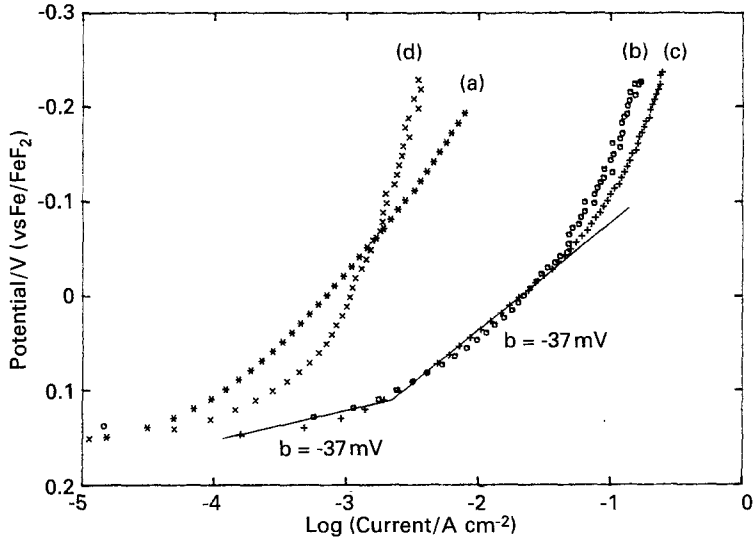

Fig. 2. Tafel plots for the HER at (a) the mild steel electrode (*), (b) for the stationary (○) and (c) 2000 r.p.m. rotating (+) porous Ni–Mo–Cd electrodes, and (d) the smooth Ni–Mo bulk alloy electrode (×) in the KF·2HF melt at 85° C.

probably arises from the large real surface area per projected cm^2 of the porous, composite Ni–Mo–Cd electrode. Factors of electronic and surface structure [16, 17], related to the exchange current density, might also be reasons when the influence of the surface area factor has been taken into account.

Secondly, at the Ni–Mo–Cd electrode, a small Tafel slope arises over the low overpotential region (η within −50 mV of the reversible potential) with $b = -37\,\text{mV}\,(\text{decade})^{-1}$ which is in good agreement with the result recorded in [2]. However, a higher slope, $b = -148\,\text{mV}\,(\text{decade})^{-1}$, is also displayed over the higher overpotential range. If the temperature effect is considered, here $T = 358\,\text{K}$, it is easily calculated from the relation of $b = 2.3RT/\beta F$ that b should be equal to 142 mV, β remaining constant (but see [15]). In this sense, the experimentally observed Tafel slope is consistent with the conventionally expected result for a discharge-controlled step.

Thirdly, erratic data points can be found at stationary Ni–Mo–Cd electrodes (○ points) in the high overpotential range, due to random growth and detachment of hydrogen bubbles generated during the polarization while the Tafel curve for a rotating Ni–Mo–Cd electrode is relatively smooth, which means rotation of the electrode assists the removal of bubbles at the surface and improves polarization performance.

Note that a current-density of ca. 200 mA cm^{-2} can be reached at a rotating Ni–Mo–Cd electrode at −0.2 V in Fig. 2, while for the smooth, mild steel electrode only 10 mA cm^{-2} can be achieved at the same potential. The Ni–Mo–Cd cathode thus provides promising performance for energy saving in practical applications of electrolysis, based on this apparent 'electrocatalytic' behaviour.

Although the alloying of Mo with Ni has been suggested by Jaksic [16] as leading to improved electrocatalysis in the HER over that at pure Ni, based on the Brewer–Engel concepts of intermetallic bonding [17], our present and earlier [8, 18] experiments do not show, at the *smooth* electrode surfaces of Ni or Ni + Mo (see Fig. 2), much advantageous effect of the presence of Mo. When Mo is coplated with Ni, as with the Ni–Mo–Cd composite coating investigated here, it is found that there is a major improvement in apparent electrocatalysis; this effect seems, however, to be mainly due to the high-area, porous nature of the coating that is generated by the electroplating procedure, with coevolution of hydrogen, rather than any striking true electrocatalytic effect (cf. [19]) arising from electronic and/or surface structure effects due to the presence of Mo in the composite coating.

Evaluation of the kinetics of the HER from the chemically analogous hydrate melt†, $KOF \cdot 2H_2O$, was also carried out in the present work, the first time such a study has been made in this medium. The $KOH \cdot 2H_2O$ melt can be treated as an intermediate system between the $KF \cdot 2HF$ melt and a dilute aqueous KOH solution so that the electrode-kinetic behaviours of Ni–Mo–Cd could be evaluated comparatively in the above media. Note that the primary discharge step in the HER from HF at a metal surface M will be $M + 2HF + e^- \rightarrow MH + FHF^-$, corresponding to the reaction $M + 2H_2O + e^- \rightarrow MH + OH^-(H_2O)$ in the aquo melt.

Figure 3 shows comparatively the Tafel plots for the Ni–Mo–Cd electrode in the $KF \cdot 2HF$ melt (+ points) and the $KOH \cdot 2H_2O$ hydrate melt (* points) at 85° C. It is interesting to observe that the cathodic current-densities in the $KOH \cdot 2H_2O$ melt are ca. 1 or 2 magnitudes *larger* than those in the $KF \cdot 2HF$ melt at corresponding overpotentials. In the polarization of Ni–Mo–Cd in the $KOH \cdot 2H_2O$ hydrate melt, the maximum current-density of ca. 3 A cm^{-2} can be reached which is much larger than that attainable practically (200 mA cm^{-2}) in the $KF \cdot 2HF$ melt, independent of differences of *IR* corrections for the two systems.

The major factor to be considered here in relation

† In the aquo-system, the chemical analogue of $KF \cdot 2HF$, in the HF-system, is $KOH \cdot 2H_2O$. Each is a di-solvate of the respective salt of the solvent anion, F^- or OH^-, and both can be regarded as low temperature 'melts'.

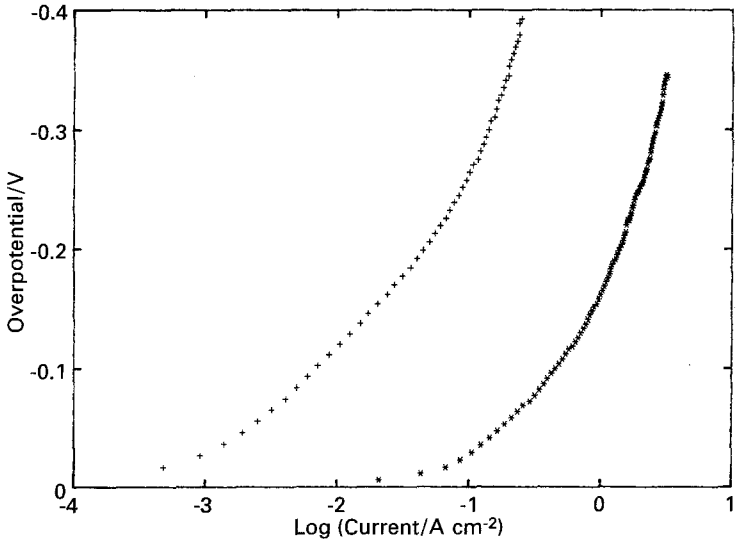

Fig. 3. Tafel plots for the HER at the Ni–Mo–Cd electrode in the KF · 2HF melt (+) and KOH · 2H$_2$O melts at 85° C.

to this substantial difference of polarization behaviour in the KF · 2HF melt in comparison with that in KOH · 2H$_2$O seems to be the microscopic accessibility of the electrode by the two electrolytes due to different wettabilities of, or contact angles of, the melts to the electrodes. Since the Ni–Mo–Cd electrode has a rough, porous structure and surface, access to the inside pores by an electrolyte or melt having high surface tension is difficult [3]. The extent of real surface of the Ni–Mo–Cd material in the KF · 2HF melt, accessible electrochemically, was therefore examined by *in situ* determination of C_{dl} from the results of the 'initial' potential-relaxation experiments. The resulting data are described in Section 5.3.

A second, electrode-kinetic factor should also be considered but may be less important than the wetting effect. In the reaction of electrochemical evolution of hydrogen from the KF · 2HF melt, the reactant, as HF, solvates the K^+ and F^- ions (the latter as FHF^-) in KF · 2HF and H_2O solvates the K^+ and OH^- ions in the KOH · 2H$_2$O melt, respectively. In general, it might be expected that discharge of H from HF would be more difficult than from H_2O (other things being equal) due to the greater electronegativity of F than O and the known and consequent larger H to F bond strength. Also the intermolecular H-bonds in H–F · · HF are stronger than those in H_2O. Both these factors, especially the H to F bond strength, would lead to more driving force, or overpotential being required to overcome the activation energy in the process of proton discharge from HF than from H_2O.

5.2. *Contact angle measurements*

The geometry and adherence of a drop or bubble at a three-phase contact is determined by Young's equation [20] which relates the surface tension values of the three interfaces (solid/liquid, solid/gas and liquid/gas) to the contact angle, evaluated here.

The Ni–Mo–Cd composite was electrolytically deposited on a flat, mild steel plate. Apparent contact angles[‡] of individual bubbles to the electrode surface were measured in the electrolyte media: KF · 2HF and KOH · 2H$_2$O at 80° C. Figures 4(a) and (b) show, respectively, the contact angle pictures made photographically at the Ni–Mo–Cd plate/H_2 bubble interfaces, within the KF · 2HF and the KOH · 2H$_2$O hydrate melts. The spherical forms are hydrogen gas bubbles while the flat-bottom parts are the surfaces of the solid Ni–Mo–Cd electroplates; both of them are in contact with the electrolyte (the bright areas). From the 'shape' of the bubbles in contact on the plate (i.e. the extent to which they are spherical), it can be seen how it is possible for the bubbles to become much more easily detached from the electrode surface when the latter is in an *aqueous* medium, than in the KF · 2HF melt, where they tend to grow larger *on* the electrode rather than become detached and displaced from the surface.

The very different measured contact angles, 44° in the KOH · 2H$_2$O hydrate melt and 78° in the KF · 2HF melt, may indicate (cf. [20]) that the surface tension of the KF · 2HF melt is higher than that of the aquo-systems. The recorded photos here are stationary images of hydrogen gas bubbles during the polarization process; their shapes may change, however, with time as more hydrogen becomes generated. A motion picture or video is relatively more vivid in revealing the practical situation, but is, of course, not available for presentation as part of this paper. However, the pictures in Fig. 4 give a good general visual impression of the momentary situation in the hydrogen-evolution process occurring at the electrode interface. The average residence time of bubbles on the surface will certainly influence the relative accessible areas of electrodes by electrolytes as also indicated from the apparent C_{dl} values derived from the initial potential-relaxation method (see below). The origin of the effect is evidently well supported

[‡] Since the Ni–Mo–Cd deposits are not microscopically smooth in comparison with a machined, polished metal surface, the reclination of bubbles at the former type of surface is microscopically different from that at smooth surfaces and the contact situation is therefore not exactly the same.

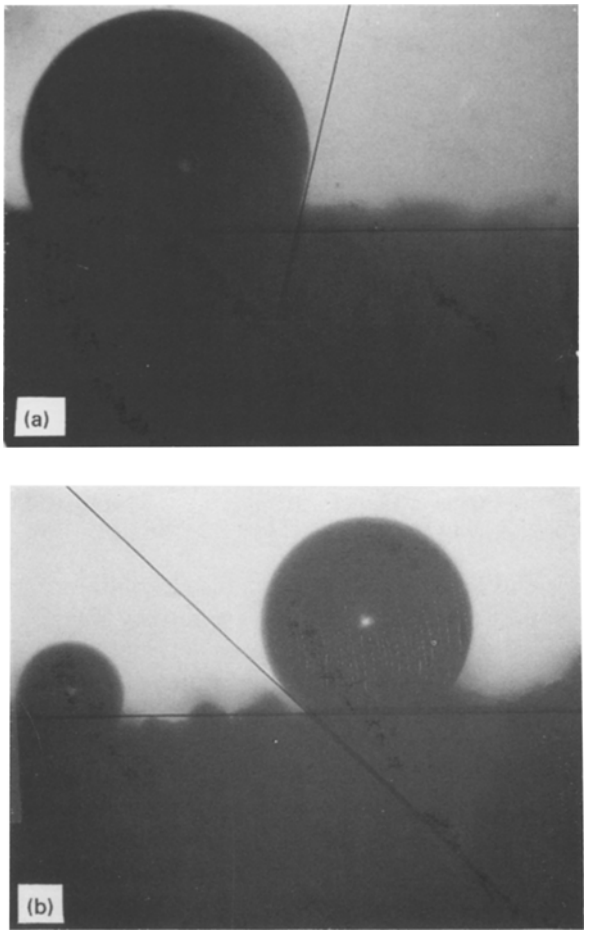

Fig. 4. (a) Contact angle, 78°, of a hydrogen bubble at the Ni–Mo–Cd electrode surface measured in the KF · 2HF melt at 80° C. (b) Contact angle, 44°, of a hydrogen bubble at the Ni–Mo–Cd electrode surface measured in the KOH · $2H_2O$ melt at 80° C.

by the present results of contact-angle measurement experiments.

5.3. *Initial potential-relaxation measurements and in situ evaluation of double-layer capacitance*

Figure 5 shows the initial potential-relaxation results (points) and the best fitted curves (as per Equation 4, solid lines) for initial current densities of (a) 214, (b) 143, (c) 107 and (d) 71.5 mA cm^{-2}, respectively, at Ni–Mo–Cd in the KF · 2HF melt. It was found that it was very difficult for the hydrogen bubbles generated at the cathode to become detached due to an unfavourable contact angle; hence a cone-shaped electrode was made as a rotating electrode (200 r.p.m.) from which hydrogen bubble detachment could be facilitated. For comparison, a smooth, bulk, Ni–Mo (94 : 6 at %) alloy electrode was used in the melt assuming a similar HER mechanism at these two electrodes.

The curve-fitting results are evidently satisfactory, following the procedure described in Section 5.1. The data for C_{dl}, thus derived for the porous Ni–Mo–Cd electrode (solid circles) in the KF · 2HF melt are shown in Fig. 6, and have an average value of $810 \pm 10\,\mu F\,cm^{-2}$, while for the smooth Ni–Mo electrode (solid box), C_{dl} had an average value of $5.9 \pm 2.0\,\mu F\,cm^{-2}$. The data for the smooth electrode were obtained preferably at high cathodic potentials. This is because high overpotentials are more easily attained at smooth electrodes than at porous electrodes under the same currents. High η values (> -100 mV) are also required for C_{dl} determination by the initial potential-relaxation method, in order to avoid (cf. [5, 13]) interference from pseudo-capacitance due to H adsorption. It is seen that the measured C_{dl} of the porous Ni–Mo–Cd electrode is *two-magnitudes* larger than that of the smooth Ni–Mo electrode in the same melt and the roughness factor of the former is calculated to be 140.

In fact, it was found that the behaviour of the porous Ni–Mo–Cd electrode in the KF · 2HF melt was not at all similar to that in the aqueous medium where the apparent C_{dl} [6] was found to be much larger than the value obtained here. A parallel experiment was carried out at this electrode in the analogue KOH · $2H_2O$ hydrate melt. The values of C_{dl}, obtained from the initial potential-relaxation measurements, are shown in Fig. 7. The gradual decrease of the measured C_{dl} with increasing cathodic potential is believed to be due to the effect of the pores being increasingly occupied by hydrogen bubbles at the expense of electrolyte. The initial potential-relaxation method measures the real area *in situ* just at

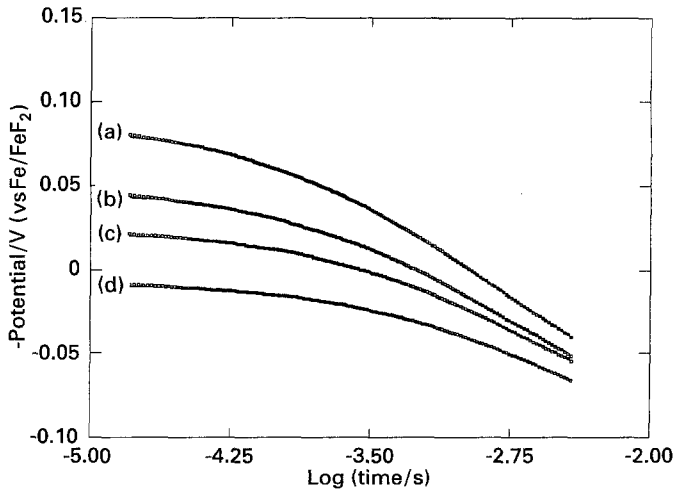

Fig. 5. Initial potential-relaxation transients for the HER at the Ni–Mo–Cd electrode in the KF · 2HF melt. $i_{t=0}$ values are (a) 214; (b) 143; (c) 107 and (d) 71.5 mA cm^{-2}, respectively. Solid lines are the best-fitted curves to the experimental data (points).

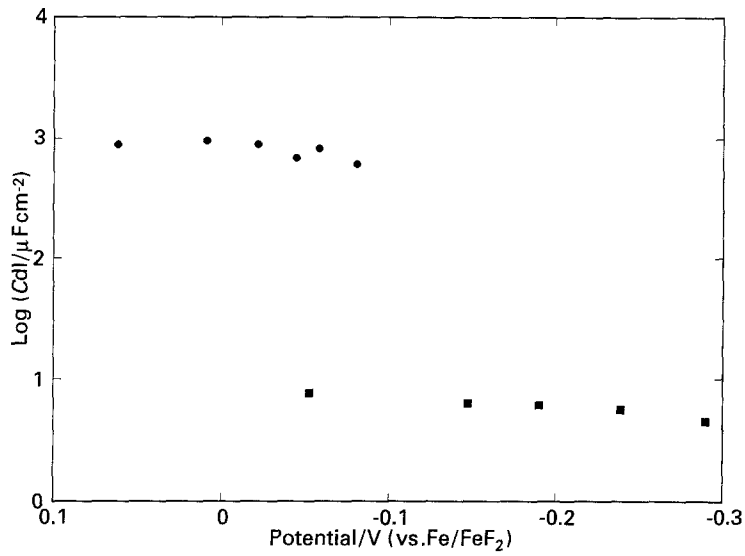

Fig. 6. Log [C_{dl}] against potential plots for the HER at the porous Ni–Mo–Cd (● points) and smooth Ni–Mo (■ points) electrodes in the KF · 2HF melt derived by means of the initial potential-relaxation method.

the moment when the current is interrupted. Thus, it reflects the *in situ* surface condition at some moment when the hydrogen gas was being evolved.

The average C_{dl} value for the Ni–Mo–Cd electrode in the KOH · $2H_2O$ melt is calculated to be $73 \pm 12\,mF\,cm^{-2}$. This is about two-magnitudes larger than the value in the KF · 2HF melt at the same electrode, over a comparative potential region, cf. Fig. 6. This interesting result indicates that, in addition to the electrode materials, the nature of electrolyte involved in the electrode process is also a factor of major importance in determining the performance in terms of apparent catalytic behaviour in electrolysis processes. Thus, the total real area of the Ni–Mo–Cd porous electrode may not be fully wetted in the fluoride melt because of the relatively high surface tension of the KF · 2HF melt and high contact angle at its interface with evolved hydrogen gas. The large difference in C_{dl} values for the fluoride and aquo (OH^-) melts cannot, we believe, be due to any intrinsic difference in the double-layer capacity in F^- and OH^- electrolytes as the interfacial properties, sizes and polarizabilities of these two ions are known to be quite similar [21].

Therefore, it can be stated that the effective porosity of an electrode material in contact with electrolyte is not an intrinsic property of a given electrode for an electrochemical reaction, but strongly depends on the accessibility of pores to the electrolyte solution and the conductivity [14] of the latter.

6. Conclusions

The following points can be made:

(i) An electrodeposited, porous Ni–Mo–Cd composite cathode material shows superior apparent electrocatalytic behaviour over that of the industrially used, mild steel for the HER from the KF · 2HF melt employed in the fluorine-production process at 85° C, because of its high surface area and probably its electronic structure as well. The high current densities attainable and low Tafel slope in the Tafel polarization behaviour characterize the good apparent electrocatalytic performance.

(ii) The electrochemically accessible real surface areas of the Ni–Mo–Cd electrode in the HER, determined *in situ* by the initial potential-relaxation method, were found to be much smaller in the KF · 2HF melt than in the analogous KOH · $2H_2O$ aquo-melt. High surface tension of the melt and unfavourable contact angle of the hydrogen bubbles at the electrode in the KF · 2HF melt limit the accessibility of the melt to the inside pores of the electrode.

(iii) Contact-angle measurements in the KF · 2HF and KOH · $2H_2O$ melts were conducted and the results support the conclusion (ii) above.

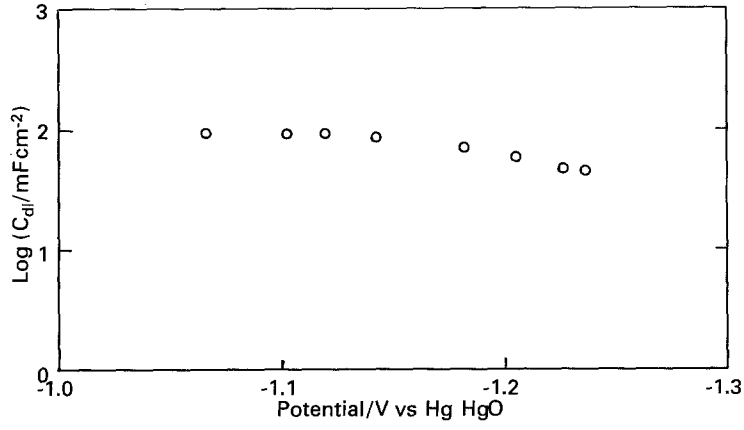

Fig. 7. Log [C_{dl}] against potential plots for the HER at the porous Ni–Mo–Cd electrode, as in Fig. 6, but for the KOH · $2H_2O$ melt, derived by means of the initial potential-relaxation method.

Acknowledgements

Grateful thanks are due to Cameco Corporation, Saskatoon, Canada and to the Natural Sciences and Engineering Research Council of Canada for financial support of this work. We also acknowledge frequent useful discussions with Dr D. G. Garratt of Cameco Corporation and Dr. T. Zawidzki during the course of the research project.

References

[1] S. Y. Qian and B. E. Conway, *J. Appl. Electrochem.*, in press (1994).
[2] B. E. Conway, H. A. Kozlowska, M. A. Sattar and B. V. Tilak, *J. Electrochem. Soc.* **130** (1983) 1825.
[3] A. J. Rudge, *in* 'Industrial Electrochemical Processes', (edited by A. T. Kuhn), Elsevier, Amsterdam (1971), Chapter 1.
[4] G. Armstrong and J. A. V. Butler, *Trans. Faraday Soc.* **29** (1933) 126.
[5] D. A. Harrington and B. E. Conway, *J. Electroanal. Chem.* **221** (1987) 1.
[6] P. Gu, L. Bai, L. Gao, R. Brousseau and B. E. Conway, *Electrochim. Acta* **37**(12) (1992) 2145.
[7] L. Gao, *Electrochem. Soc., Interface* **2**(3), (1993) p. 7.
[8] B. E. Conway and L. Bai, *J. Chem. Soc. Faraday Trans.* **81**(1) (1984) 1841.
[9] J. O'M. Bockris and S. Srinivasan, in 'Fuel Cells: Their Electrochemistry', McGraw-Hill, New York (1969), Chapter 5.
[10] R. de Levie, *in* 'Advances in Electrochemistry and Electrochemical Engineering', vol. 6, (edited by P. Delahay), Interscience, New York (1964) pp 56–124.
[11] R. Parsons and F. R. G. Zobel, *J. Electroanal. Chem.* **9** (1965) 333.
[12] B. E. Conway and E. Gileadi, *Trans. Faraday Soc.* **58** (1962) 2493.
[13] L. Bai, L. Gao and B. E. Conway, *J. Chem. Soc., Faraday Trans* **89**(2) (1993) 235.
[14] *Idem, ibid.* **89**(2), (1993) 243.
[15] B. E. Conway, *Modern Aspects of Electrochemistry* **18** (1986) 103.
[16] M. Jaksic, *Intl. J. Hydrogen Energy* **11** (1986) 519; see also *Mat. Chem. Phys.* **22** (1989) 1.
[17] L. Brewer, *Science* **161** (1968) 115.
[18] B. E. Conway and R. Brousseau, in course of publication (1994); see R. Brousseau, PhD thesis, University of Ottawa (1990).
[19] B. E. Conway and B. V. Tilak, *Adv. in Catalysis* **38** (1992) 1.
[20] T. Young, *Phil. Trans. Roy. Soc. London*, (1805) p. 84.
[21] D. C. Grahame, *Chem. Rev.* **41** (1947) 441.